Disease-associated mutations affect intracellular traffic and paracellular Mg^{2+} transport function of Claudin-16

P. Jaya Kausalya,[1] Salah Amasheh,[2] Dorothee Günzel,[2] Henrik Wurps,[2] Dominik Müller,[3] Michael Fromm,[2] and Walter Hunziker[1]

[1]Epithelial Cell Biology Laboratory, Institute of Molecular and Cell Biology, Singapore. [2]Department of Clinical Physiology, Charité, Campus Benjamin Franklin, and [3]Department of Pediatric Nephrology and Center for Cardiovascular Research, Charité, Berlin, Germany.

Claudin-16 (Cldn16) is selectively expressed at tight junctions (TJs) of renal epithelial cells of the thick ascending limb of Henle's loop, where it plays a central role in the reabsorption of divalent cations. Over 20 different mutations in the *CLDN16* gene have been identified in patients with familial hypomagnesemia with hypercalciuria and nephrocalcinosis (FHHNC), a disease of excessive renal Mg^{2+} and Ca^{2+} excretion. Here we show that disease-causing mutations can lead to the intracellular retention of Cldn16 or affect its capacity to facilitate paracellular Mg^{2+} transport. Nine of the 21 Cldn16 mutants we characterized were retained in the endoplasmic reticulum, where they underwent proteasomal degradation. Three mutants accumulated in the Golgi complex. Two mutants were efficiently delivered to lysosomes, one via clathrin-mediated endocytosis following transport to the cell surface and the other without appearing on the plasma membrane. The remaining 7 mutants localized to TJs, and 4 were found to be defective in paracellular Mg^{2+} transport. We demonstrate that pharmacological chaperones rescued surface expression of several retained Cldn16 mutants. We conclude that FHHNC can result from mutations in Cldn16 that affect intracellular trafficking or paracellular Mg^{2+} permeability. Knowledge of the molecular defects associated with disease-causing Cldn16 mutations may open new venues for therapeutic intervention.

Introduction

Hypercalciuria is a major determinant of calcium-related kidney stone diseases and nephrocalcinosis (1). The etiology of hypercalciuria is heterogeneous, as it may be caused by various underlying disorders. One such disorder, familial hypomagnesemia with hypercalciuria and nephrocalcinosis (FHHNC; OMIM 248250), is characterized by progressive renal Ca^{2+} and Mg^{2+} wasting, leading to impaired renal function and, in most cases, chronic renal failure around the time of diagnosis (2, 3). FHHNC is caused by mutations in the *claudin 16* (*Cldn16*) gene, previously known as *paracellin-1* (4, 5), encoding the Cldn16 protein.

Cldn16 is a member of a family of transmembrane proteins that constitute the intercellular tight junction (TJ) barrier in various epithelia (6). Claudins span the plasma membrane 4 times, with their N and C termini located in the cytosol. Most claudins encode a C-terminal postsynaptic density 95/discs large/zonula occludens-1 (PDZ) domain–binding motif that can interact with PDZ domain scaffolding proteins such as the zonula occludens (ZO) proteins (7). The 2 luminal loops mediate homo- and/or heterotypic interactions with claudins on neighboring cells (8). Besides a postulated role in cell-cell adhesion, claudins function as paracellular ion channels that either facilitate or restrict the paracellular diffusion of selective ions (9, 10). The characteristic ion permeability of an epithelium is thus thought to reflect to a significant extent its repertoire in claudin molecules. Cldn16 expression is restricted to the thick ascending part of the loop of Henle in the kidney, where it is believed to form paracellular channels that allow the reabsorption of Mg^{2+} and Ca^{2+}, a process basically driven by an electrochemical gradient (4). Consequently, patients suffering from FHHNC experience severe renal Mg^{2+} and Ca^{2+} loss, eventually resulting in renal failure.

To date, over 20 different mutations in *Cldn16* have been associated with FHHNC (2–5, 11) (Figure 1). With a single exception (11), these mutations affect either 1 of the 4 transmembrane domains or 1 of the 2 extracellular loops of the molecule. Although it has been suggested that these mutations might interfere with the capacity of Cldn16 to transport Mg^{2+} and Ca^{2+} ions (4), the underlying molecular mechanisms have begun to be unraveled only recently (11, 12). T233R, a Cldn16 mutation associated with a self-limiting form of childhood hypercalciuria, has recently been shown to inactivate the PDZ-binding motif in Cldn16, abolish its binding to ZO-1, and lead to its lysosomal mislocalization (11). A recent study correlated Cldn16 expression with increased permeability of TJs to Na^+, indicating that Cldn16 helps in maintaining the electrochemical gradient thought to drive Mg^{2+} reabsorption in the loop of Henle (12).

Here we provide insight into the molecular mechanism by which the 21 mutations linked to FHHNC described to date affect Cldn16 function. These mutations can be classified into 2 categories, depending on whether they interfere with the correct intracellular trafficking of Cldn16 or its paracellular Mg^{2+} transport function. Mutant Cldn16 molecules belonging to the first category accumulate in different intracellular compartments of

Nonstandard abbreviations used: AAS, atomic absorption spectrometry; ALLN, N-acetyl–leu-leu-norleucinal; CFTR, cystic fibrosis transmembrane conductance regulator; Cldn, claudin; EEA1, early endosome antigen 1; FHHNC, familial hypomagnesemia with hypercalciuria and nephrocalcinosis; MDCK, Madin-Darby canine kidney; 4-PBA, 4-phenylbutyrate; $P_{Mg^{2+}}$, Mg^{2+} permeability; P_{Na}/P_{Cl} ratio, sodium permeability/chloride permeability ratio; R^t, transepithelial electrical resistance; TGN, trans-Golgi network; TJ, tight junction; ZO, zonula occludens.

Conflict of interest: The authors have declared that no conflict of interest exists.

Citation for this article: *J. Clin. Invest.* **116**:878–891 (2006). doi:10.1172/JCI26323.

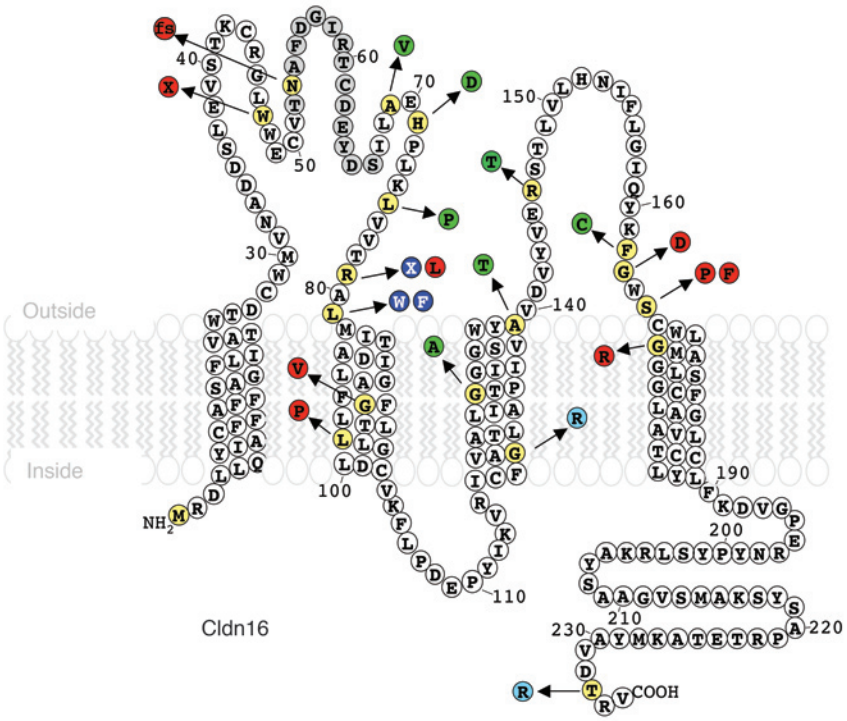

Figure 1
Predicted topology of Cldn16 and location of the different mutations linked to FHHNC reported. Shown is the amino acid sequence in 1-letter code, with mutated residues in yellow and arrows indicating the change introduced by the mutation. The effect of the corresponding mutation on the predominant steady-state distribution of Cldn16 is highlighted in different colors: green, cell surface; red, ER; dark blue, Golgi complex; light blue, lysosomes. X, stop codon, fs, frame shift. The peptide (T52-S66) used to generate the anti-loop antibody is shaded in gray.

the exocytic and/or endocytic pathways and are therefore absent from — or only transiently expressed on — the cell surface. Here we demonstrate that increased surface expression of some of these Cldn16 mutants can be rescued using pharmacological chaperones. The second category is composed of Cldn16 mutants that are correctly delivered to the TJ but are defective in Mg^{2+} permeability ($P_{Mg^{2+}}$). Our results provide insight into pathophysiology and putative therapies of human Cldn16 defects.

Results

Characterization of an antibody to the first extracellular loop of Cldn16. To monitor cell surface expression and internalization of Cldn16, we generated an anti-peptide antibody to the first extracellular loop of the protein (amino acids T52–S66; Figure 1). To test the antibody, control Madin-Darby canine kidney (MDCK) and HeLa cells or cells expressing HA-tagged Cldn16 were incubated with the affinity-purified anti-loop antibody at 4°C or 37°C, and cell-associated anti-loop antibody was detected by immunofluorescence staining. While no bound anti-loop antibody was detected in MDCK cells incubated at 4°C (data not shown), it was present at regions of cell-cell contact as well as in intracellular vesicles of cells incubated at 37°C (Figure 2A), suggesting that the antibody was endocytosed. Antibody staining was blocked by the presence of antigenic peptide (Figure 2B), and no staining was observed with the preimmune serum (Figure 2C), establishing the specificity of the antibody and indicating that MDCK cells express Cldn16 endogenously. These controls also establish that internalization of the antibody at 37°C did not occur via fluid-phase endocytosis, but most likely following its binding to Cldn16 present on the cell surface. Similar results were obtained for MDCK cells transfected with a cDNA for HA-tagged Cldn16 (11), where cell surface and vesicular staining was observed when the anti-loop antibody was present at 37°C (Figure 2, D–F). As expected, the labeling for the HA tag (Figure 2D) and the anti-loop antibody (Figure 2E) extensively overlapped (Figure 2F), probably representing Cldn16 molecules that had been exposed on the cell surface, whereas Cldn16 molecules only labeled with the anti-HA antibody likely represent molecules in transit in different compartments of the biosynthetic pathway.

The anti-loop antibody did not stain HeLa cells, consistent with the absence of endogenous Cldn16 (see Figure 3V). Only faint cell surface labeling was observed in Cldn16-expressing HeLa cells incubated with the anti-loop antibody at 37°C, and the bulk of the staining for either Cldn16 (Figure 2L) or the anti-loop antibody (Figure 2G) was vesicular, which suggests that in these cells, Cldn16 may not be retained in the plasma membrane. In contrast to renal epithelial MDCK cells with a well-established capacity to polarize and form functional TJs, HeLa cells are derived from a cervical carcinoma, are less polarized, and only express low levels of the TJ protein ZO-1 (data not shown), which is known to interact with Cldn16 (11). No staining was observed when either control or transfected MDCK and HeLa cells were incubated with the anti-loop antibody at 4°C or when cells were fixed prior to staining (data not shown), possibly reflecting a restricted accessibility of the epitope at low temperature and/or sensitivity to fixation.

In sum, an anti-loop antibody was generated as a tool to detect the appearance of Cldn16 on the cell surface and analyze its ability to endocytose.

Cldn16 is internalized via a clathrin-dependent pathway. To confirm that Cldn16 is endocytosed, we sought to determine whether Cldn16 is delivered to early endosomes and whether internalization occurs via a clathrin- or caveolae-dependent mechanism. To determine whether Cldn16 is delivered to early endosomes, HeLa cells expressing HA-tagged Cldn16 were allowed to internalize anti-loop antibody at 37°C. The anti-loop antibody and early endosomes were then immunolabeled and visualized by confocal immunofluorescence microscopy. As shown in Figure 2, G–I, the anti-loop antibody internalized via Cldn16 (Figure 2G) extensively colocalized with the early endosomal marker early endosome antigen 1 (EEA1; Figure 2, H and I). Likewise, Cldn16 itself stained with the anti-HA antibody colocalized with EEA1 (Figure 2L).

To determine whether Cldn16 internalizes via a clathrin- or caveolae-dependent pathway, HeLa cells expressing HA-tagged Cldn16 were incubated with anti-loop antibodies at 37°C and subjected to different experimental conditions that selectively affect clathrin-

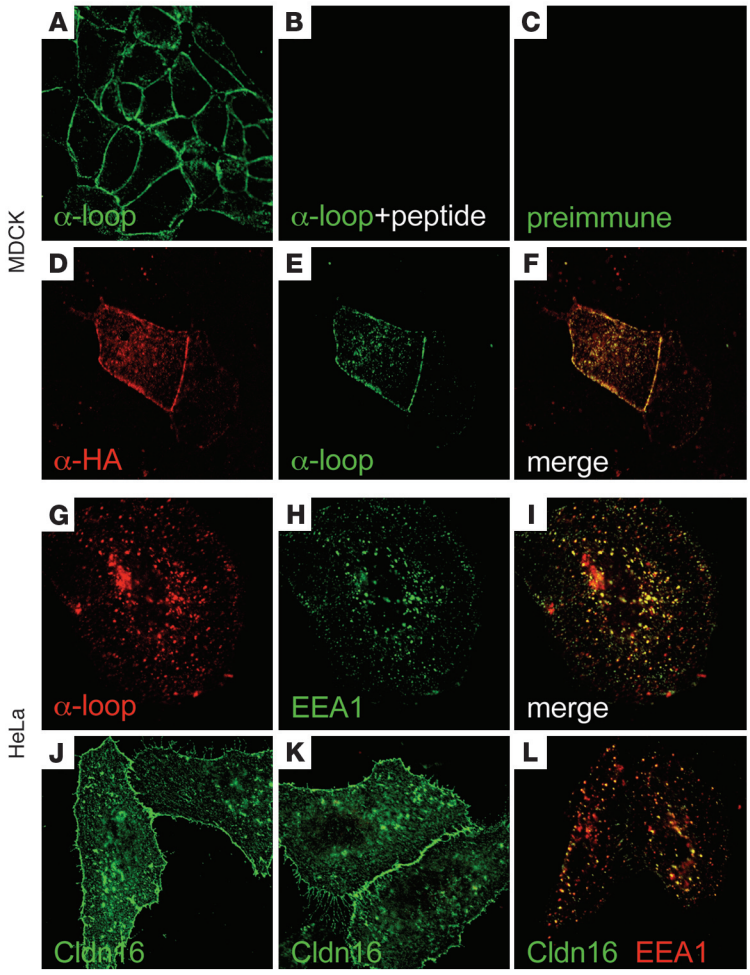

Figure 2
Clathrin-mediated endocytosis of Cldn16. (**A**–**C**) Characterization of an antibody to the first extracellular loop of Cldn16 (α-loop) and endogenous Cldn16 expression in MDCK cells. MDCK cells were incubated for 1 hour at 37°C in the presence of anti-loop antibody alone (**A**), together with antigenic peptide (**B**), or with preimmune serum (**C**). Cells were then washed, fixed, and permeabilized, and the anti-loop antibody was detected by immunofluorescence microscopy using a labeled secondary antibody. (**D**–**F**) Detection of HA-tagged Cldn16 expressed in MDCK cells. MDCK cells expressing N-terminally HA epitope–tagged Cldn16 were incubated for 1 hour at 37°C with anti-loop antibody. α-HA (**D**) and the anti-loop antibody (**E**) were then detected in permeabilized cells. (**F**) Merging the HA and anti-loop antibody staining shows extensive colocalization at the cell surface and in a few intracellular vesicles. (**G**–**I**) Detection of anti-loop antibody internalized via HA-tagged Cldn16 in early endosomes of transfected HeLa cells. Anti-loop antibody (**G**) and EEA1 (**H**) were visualized by immunofluorescence microscopy, and the 2 images were merged (**I**). (**J**–**L**) Clathrin-mediated internalization of Cldn16. HeLa cells expressing HA-tagged Cldn16 were incubated for 1 hour at 37°C with anti-loop antibody under either hypertonic (**J**) or cytosol acidified (**K**) conditions to disrupt clathrin function or in the presence of cholesterol oxidase (**L**) to disrupt caveolae. Cldn16 was then visualized by immunofluorescence microscopy. In **L**, cells were stained with antibodies to EEA1, and the merged image is shown. Shown are representative images of 2–3 independent experiments.

and/or caveolae-mediated internalization. Transient expression of a dominant inactive form of dynamin 1, which can block both clathrin- and caveolae-dependent internalization (13–15), resulted in a significant accumulation of Cldn16 on the cell surface compared with control cells or cells expressing WT dynamin (our unpublished observations). Hypertonic media and cytosol acidification, which selectively block clathrin-mediated endocytosis (16, 17), resulted in the accumulation of Cldn16 on the plasma membrane (Figure 2, compare G and L to J and K). In contrast, cholesterol oxidase, a selective inhibitor of caveolae-mediated uptake (18, 19), did not interfere with the internalization of Cldn16 to early endosomes (Figure 2L).

Cldn16 mutants differ in their capacity to be expressed on the cell surface. To analyze the subcellular steady-state localization of the different mutant Cldn16 proteins identified in patients with FHHNC (Figure 1), cells expressing the different HA-tagged mutants were incubated in the presence of the anti-loop antibody for 1 hour at 37°C, fixed, and permeabilized, and Cldn16 as well as the anti-loop antibody were localized by confocal laser scanning microscopy. Monitoring of the binding and internalization of anti-loop antibody by live cells provides a sensitive assay to monitor cell surface exposure, even if transient in nature, of integral membrane proteins (20). However, since the anti-loop antibody binds to untransfected MDCK cells (see above), HeLa cells had to be used.

Several Cldn16 mutants, in particular W47X (Figure 3A), N53fs (Figure 3B), R79X (Figure 3G), L81F (Figure 3H), L81W (Figure 3I), G92V (Figure 3J), L97P (Figure 3K), G121R (Figure 3L), G163D (Figure 3Q), S165F (Figure 3R), and S165P (Figure 3S), showed predominant intracellular localization and could not be detected on the cell surface as evidenced by the absence of anti-loop antibody staining. These mutants also failed to internalize the anti-loop antibody, indicating that they were not exposed, even transiently, on the cell surface. With the exception of W47X and N53fs, which were not expected to bind the anti-loop antibody (Figure 1), the other mutants are likely to be recognized by the antibody, given that it can detect A62V, H71D, and L75P (Figure 3, C, D, and F), where the mutations are located in close vicinity to the epitope (Figure 1). Similar intracellular localization for the above Cldn16 mutants was also observed in MDCK cells (see below).

A62V, H71D, L75P, G128A, A139T, R146T, F162C, R79L, G169R, and T233R (Figure 3, C–F, M–P, T, and U) also displayed predominant intracellular localization, but they did internalize the anti-loop antibody, consistent with transient exposure on the cell surface. With the exception of R79L, G169R (see below), and T233R (11), which retained predominant intracellular localization, these mutants were enriched on the cell surface in MDCK cells, where they colocalized with ZO-1 at TJs (see below). Untransfected control cells showed no staining (Figure 3V), confirming the specificity of the staining for the HA-tagged Cldn16 mutants and the anti-loop antibodies.

In sum, several mutations linked to FHHNC affect the normal cell surface expression of Cldn16, presumably reflecting defects

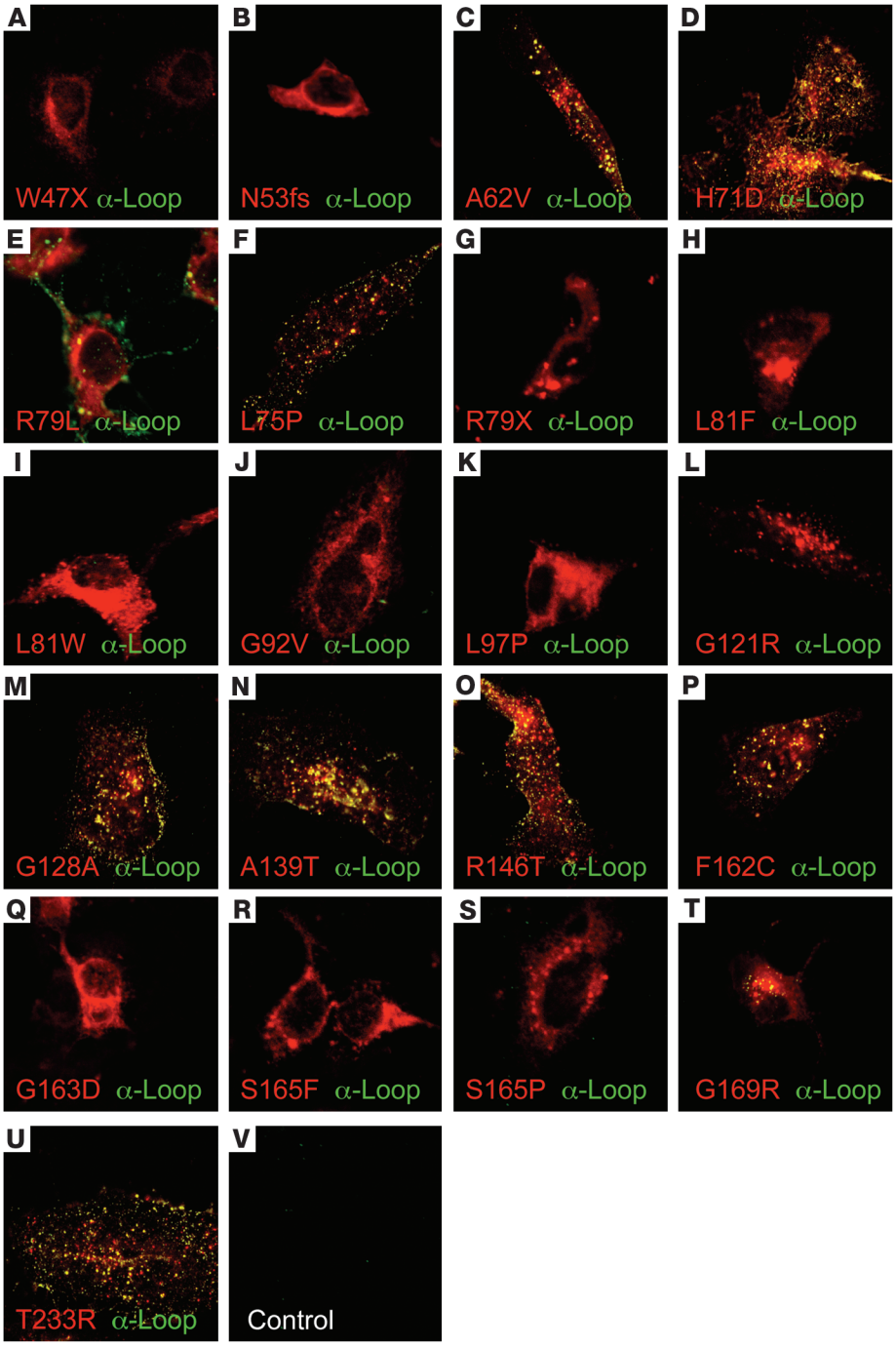

Figure 3
Cell surface expression of Cldn16 mutants linked to FHHNC. HeLa cells transiently expressing the indicated HA-tagged Cldn16 mutants were incubated in the presence of anti-loop antibody for 1 hour at 37°C and then immunostained to detect the HA tag (red) or the anti-loop antibody (green). Merged images are shown. Shown are representative images of 2–3 independent experiments.

in intracellular trafficking at different steps of the biosynthetic and/or endocytic pathways.

Cldn16 mutants that fail to reach the cell surface localize either to the ER, the Golgi complex, or lysosomes. To identify compartments to which Cldn16 mutants with predominant intracellular steady-state distribution localize, we carried out colocalization experiments in transfected MDCK and HeLa cells with markers for the ER (calreticulin, ref. 21), the Golgi complex (GM130, ref. 22) and lysosomes (CD63, ref. 23; Lamp2, ref. 20). N53fs extensively colocalized with calreticulin, both in MDCK (Figure 4, A–C) and HeLa (Figure 4, D–F) cells. Other mutants showing an extensive ER localization were W47X, R79L, R79X, L81F, L81W, G92V, L97P, G121R, G163D, S165F, S165P, and G169R (Supplemental Figure 1; supplemental material available online with this article; doi:10.1172/JCI26323DS1). In contrast, T233R and WT Cldn16 (Supplemental Figure 1) as well as A62V, H71D, L75P, G128A, A139T, R146T, and F162C (data not shown) showed little or only partial overlap with calreticulin. Of the mutants showing predominant intracellular localization, R79X extensively colocalized with the Golgi marker GM130, both in MDCK (Figure 4, G–I) and HeLa cells (Figure 4, J–L), as did L81F, L81W, and G121R (see Supplemental Figure 1).

Besides T233R, which has previously been shown to localize to lysosomes in MDCK cells (11) and also colocalized Lamp2 in MDCK (Figure 4, P–R) and with CD63 in HeLa (Figure 4, V–X) cells, one additional mutant, G121R, was readily detected in Lamp2- or CD63-positive vesicular structures in MDCK (Figure 4, M–O) and HeLa (Figure 4, S–U) cells, respectively.

In sum, Cldn16 mutants that fail to appear on the cell surface localize to different intracellular compartments at equilibrium.

Characterization of trafficking defects of Cldn16 mutants displaying predominant intracellular steady-state localization. In addition to the predominant localization to a particular intracellular compartment at equilibrium as described above, several Cldn16 mutants were also detected, to varying extents, in other organelles (see Table 1). For example, in addition to the ER, G169R was also detected in the Golgi complex (data not shown) and, in MDCK cells, the cell surface (see below). R79X, L81F and L81W, which predominantly localized to the Golgi complex, were also detected in lysosomes (see below). The mainly lysosomal G121R was also detected in the ER and the Golgi complex (Table 1). To further characterize the trafficking defects associated with the different intracellular Cldn16 mutants, we incubated cells at 20°C, conditions that block the exit of proteins from the Golgi complex and

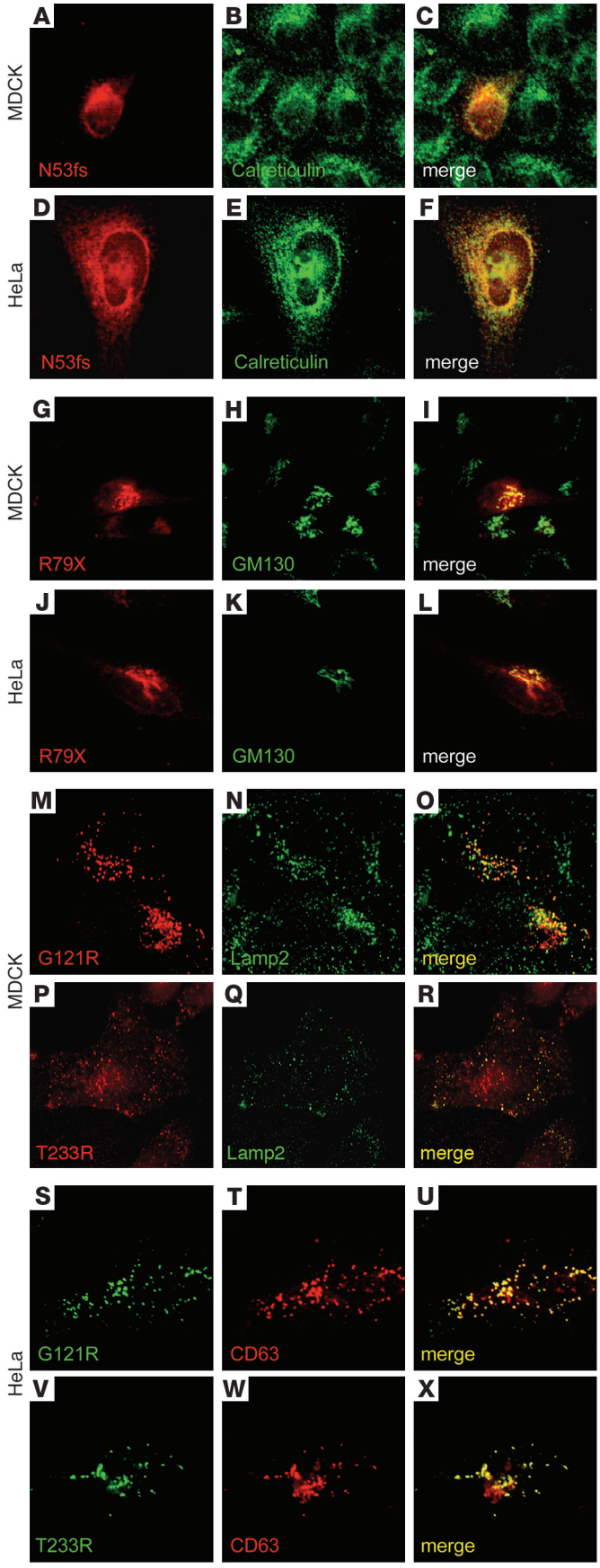

Figure 4
Steady-state localization of selected Cldn16 mutants to different subcellular organelles. (**A**–**F**) Example of a representative mutant with predominant ER localization. MDCK or HeLa cells expressing HA-tagged N53fs were immunostained for HA (**A** and **D**, red) and the ER marker calreticulin (**B** and **E**, green). Colocalization was apparent in the merged images (**C** and **F**, yellow). (**G**–**L**) Representative mutant with predominant Golgi localization. MDCK or HeLa cells expressing HA-tagged R79X were immunostained for HA (**G** and **J**, red) and the Golgi marker GM130 (**H** and **K**, green). Colocalization was apparent in the merged images (**I** and **L**, yellow). (**M**–**X**) Mutants with predominant lysosomal localization. MDCK or HeLa cells expressing HA-tagged G121R or T233R were immunostained for HA (**M** and **P**, red, and **S** and **V**, green) and the lysosome markers Lamp2 (**N** and **Q**, green) or CD63 (**T** and **W**, red). Colocalization was apparent in the merged images (**O**, **R**, **U**, and **X**, yellow). Shown are representative images of 2–3 independent experiments. For the remaining mutants, see Supplemental Figure 1.

trans-Golgi network (TGN) (24, 25). Cldn16 mutants were then analyzed for their colocalization with GM130 (Figure 5, A and D). If a particular Cldn16 mutant failed to exit the ER, it was expected not to colocalize with the Golgi marker under these conditions. Alternatively, following the 20°C incubation, protein synthesis and degradation were inhibited with cycloheximide and N-acetyl-leu-leu-norleucinal (ALLN), respectively, and cells were shifted to 37°C prior to staining for GM130 (Figure 5, B and E) or CD63 (Figure 5, C and F). This experiment determines whether a particular Cldn16 mutant is retained in the Golgi complex or exits the Golgi complex to be delivered to lysosomes.

L97P did not colocalize with GM130 following the 20°C incubation (Figure 5A) and, as expected, colocalized neither with GM130 (Figure 5B) nor with CD63 (Figure 5C) after release from the 20°C block. Similar behavior was observed for W47X, N53fs, R79L, G92V, G163D, S165F, and S165P (see Supplemental Figure 2), all of which displayed predominant ER equilibrium localization. These results strongly indicate that these mutants are unable to exit the ER. In contrast, G121R extensively colocalized with GM130 at 20°C (Figure 5D). Interestingly, following release from the 20°C block, a significant fraction of this mutant no longer colocalized with GM130 (Figure 5E) and appeared in a vesicular compartment positive for CD63 (Figure 5F). Similar distribution was found for R79X, L81F, and L81W (see Supplemental Figure 2), which, like G121R, showed predominant Golgi equilibrium localization. Thus, although these mutants show predominant Golgi localization at equilibrium, they can exit the Golgi complex and reach lysosomes.

In sum, Cldn16 mutants that display predominant intracellular equilibrium localizations are either retained in the ER or delivered to the Golgi complex and lysosomes.

Cldn16 mutants retained in the ER are subject to proteasomal degradation. We next determined whether Cldn16 mutants that are retained in the ER are targeted for proteasomal degradation by the ER quality-control machinery. HeLa cells expressing WT Cldn16 or different mutants were incubated in the absence or presence of the proteasome inhibitor ALLN (26) for 10 hours and then stained with antibodies to HA and ubiquitin (Figure 6, A–F). Little ubiquitin was detected in cells expressing Cldn16, and in the presence of ALLN, ubiquitin staining did not increase significantly and did not colocalize with Cldn16 (Figure 6, A and D). In contrast, cells expressing N53fs (Figure 6, B and E), as well

Table 1
Summary of steady-state localization and defects of Cldn16 mutants linked to FHHNC

	Surface	ER	Golgi	Lysosomes	Defect	Rescue
Cldn16	+				-	
W47X		+			ER exit	
N53fs		+			ER exit	
A62V	+				Mg^{2+} transport?	
H71D	+				Mg^{2+} transport	
L75P	+				Mg^{2+} transport	
R79X		+	+[A]	+	Lysosomal delivery	
R79L	+	+[A]			ER exit (partial)	Thaps
L81W		+	+[A]	+	Lysosomal delivery	
L81F		+	+[A]	+	Lysosomal delivery	
L97P		+			ER exit	
G92V		+			ER exit	
G121R		+[A]	+	+[A]	Lysosomal delivery	Thaps/4-PBA
G128A	+				Mg^{2+} transport	
A139T	+				Mg^{2+} transport?	
R146T	+				Mg^{2+} transport	
F162C	+				Mg^{2+} transport?	
G163D		+			ER exit	
S165F		+			ER exit	
S165P		+			ER exit	
G169R	+	+[A]			ER exit (partial)	Thaps/4-PBA
T233R	+			+[A]	Lysosomal delivery/ Mg^{2+} transport?	

[A]Predominant steady-state localization. Thaps, thapsigargin. Possible defects in Ca^{2+} transport were not analyzed in this study.

as W47X, R79L, G92V, G163G, S165F, and S165P (see Supplemental Figure 3), which are all retained in the ER, showed increased ubiquitin labeling that was further enhanced in the presence of ALLN and extensively colocalized with the corresponding Cldn16 mutants. Mutants with predominant Golgi and partial ER localization (i.e., R79X, L81F, L81W and G121R) also showed increased colocalization with ubiquitin in the presence of ALLN (see Supplemental Figure 3). T233R, which is predominantly found in lysosomes, did not colocalize with ubiquitin (Figure 6, C and F).

These data, which suggest that Cldn16 mutants that are retained in the ER are ubiquitinated and degraded by the proteasome, was corroborated biochemically. We incubated HEK-293T cells transiently expressing WT Cldn16 or selected mutants for 6 hours in the presence or absence of ALLN, and Cldn16 protein levels were determined by Western blot analysis. As shown in Figure 6G, inhibiting proteasomal degradation did not significantly alter protein levels for WT Cldn16, mutants that are transported to the cell surface (i.e., A139T), or lysosomes (i.e., T233R). In contrast, the ER retained G92V, R79L, L97P, G163D, S165F, and S165P accumulated in the presence of ALLN, consistent with these mutants being subject to proteasomal degradation under normal conditions. G121R, which is predominant in lysosomes at equilibrium but can also be detected in the ER, was moderately stabilized by ALLN.

To further substantiate these data, 293T cells expressing Cldn16 or G92V were treated with cycloheximide to inhibit de novo protein synthesis (27), and Cldn16 protein levels were monitored every 2 hours by Western blot analysis. Only 25% of the Cldn16 initially present was detected in cells treated for 10 hours with cycloheximide, and the addition of ALLN only led to a modest stabilization (Figure 6H). In contrast, the ER-retained G92V turned over more rapidly than did WT Cldn16, and its turnover was blocked by ALLN.

Cldn16 mutants delivered to lysosomes take different routes. T233R and G121R showed extensive lysosomal steady-state localization. Lysosomal delivery of newly synthesized membrane proteins can occur either directly from the Golgi complex via endosomes or indirectly following delivery to the plasma membrane and internalization (28). To analyze by which of the 2 routes T233R and G121R reach lysosomes, we determined whether live HeLa cells expressing the 2 mutants are able to bind and internalize anti-loop antibodies added to the medium at 37°C.

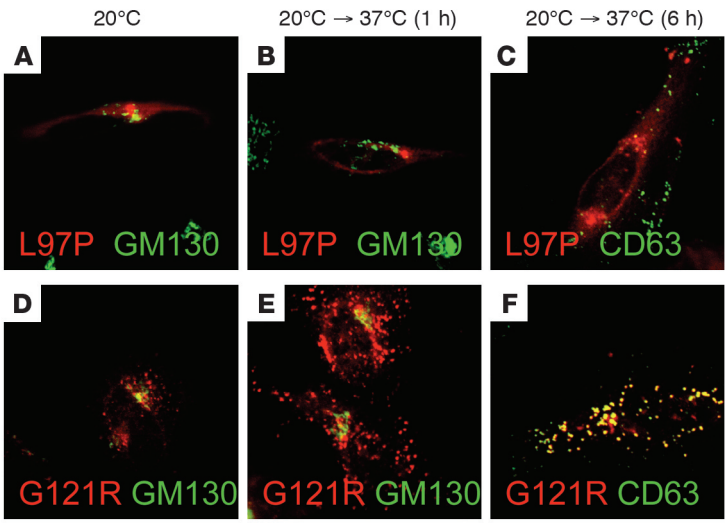

Figure 5
Characterization of intracellular trafficking defects of representative Cldn16 mutants. Transfected MDCK cells expressing the indicated HA-tagged Cldn16 mutants were incubated at 20°C for 3 hours to allow transport out of the ER but prevent exit from the Golgi complex and TGN. Cells were then either processed for immunofluorescence staining (**A** and **D**) or transferred to 37°C for 1 hour (**B** and **E**) or 6 hours (**C** and **F**) in the presence of cycloheximide and ALLN to inhibit de novo protein synthesis and degradation, respectively. The cells were then immunostained with antibodies to HA to detect the tagged Cldn16 mutant (red) and either the Golgi marker GM130 (**A**, **B**, **D**, and **E**, green) or the lysosomal membrane protein CD63 (**C** and **F**, green). Shown are representative images of 2–3 independent experiments. For the remaining mutants, see Supplemental Figure 2.

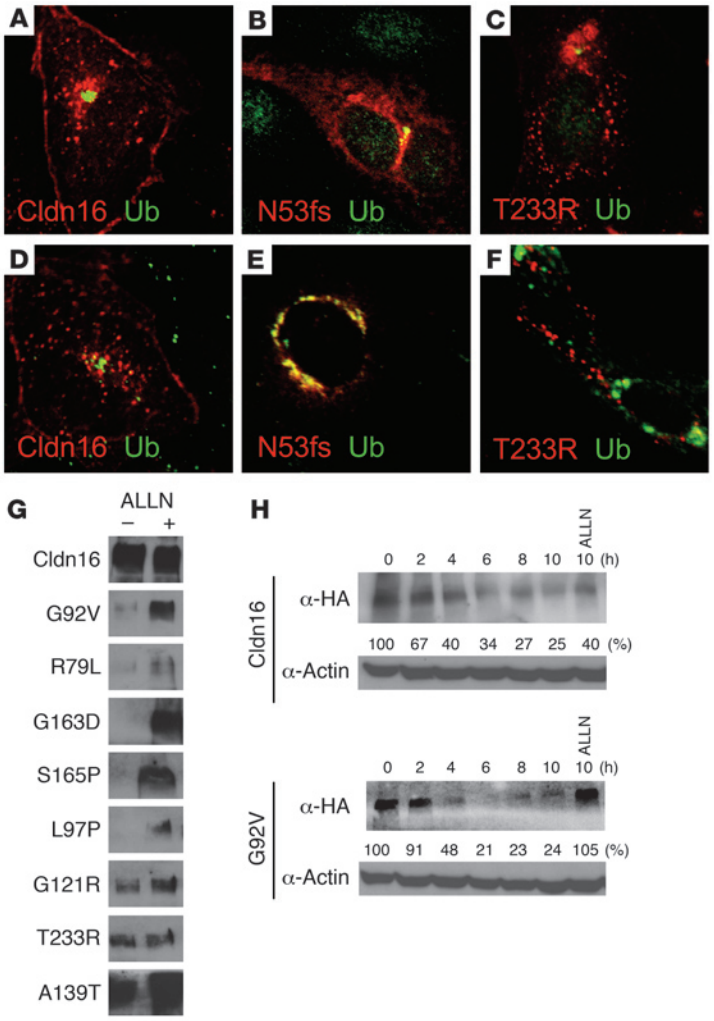

Figure 6
ER-retained Cldn16 mutants are subject to proteasomal degradation. (**A**–**F**) Colocalization of ER-retained Cldn16 mutants with ubiquitin was increased in the presence of a proteasome inhibitor. Transfected MDCK cells expressing HA-tagged Cldn16 or the indicated mutants were incubated for 10 hours in the absence (**A**–**C**) or presence (**D**–**F**) of the proteasome inhibitor ALLN. Cells were then immunostained with antibodies to detect the HA-tagged Cldn16 mutant (red) or ubiquitin (Ub, green). Colocalization was apparent in the merged images (yellow). Shown are representative images of 2–3 independent experiments. For the remaining mutants, see Supplemental Figure 3. (**G**) ER-retained Cldn16 mutants were stabilized by proteasome inhibitors. HEK-293T cells transiently expressing the indicated HA-tagged Cldn16 mutants were incubated in the absence (–) or presence (+) of the proteasome inhibitor ALLN. Cells were then lysed, and Cldn16 was detected by SDS-PAGE and Western blot analysis. Blotting for actin was used as a loading control (data not shown). (**H**) Turnover of ER-retained Cldn16 mutants was blocked by proteasome inhibitors. HEK-293T cells transiently expressing HA-tagged Cldn16 or the ER-retained HA-tagged G92V were cultured in cycloheximide to block de novo protein synthesis for the time periods indicated, either in the absence or presence of the proteasome inhibitor ALLN. Cells were then lysed, and Cldn16 detected by SDS-PAGE and Western blot analysis. Percent expression relative to that at 0 hours is shown below each lane. Blotting for actin was used as a loading control. One representative blot and quantification of 3 independent experiments is shown.

Cells expressing T233R efficiently internalized anti-loop antibodies and extensively colocalized with the lysosomal marker CD63 (Figure 7, A–C), indicating that T233R was exposed on the cell surface prior to being internalized and transported to lysosomes. In contrast, cells expressing G121R failed to internalize anti-loop antibodies (Figure 7, G–I). To exclude the possibility that G121R failed to bind anti-loop antibodies due to a shorter residence time on the cell surface compared with T233R, endocytosis was blocked using cytosol acidification (see above). Under these conditions, the anti-loop antibody stained the cell surface of cells expressing T233R and was no longer transferred to lysosomes (Figure 7, D–F), confirming that T233R transits through the plasma membrane before reaching lysosomes. In contrast, no anti-loop antibody was detected on the surface of cells expressing G121R, even when internalization was blocked (Figure 7, J–L), consistent with a direct transport to lysosomes.

Cells expressing R79X, L81F, and L81W, which were delivered from the Golgi complex to lysosomes following release from the 20°C block (see above), did not internalize anti-loop antibodies. These mutants also could not be detected on the cell surface when endocytosis was inhibited (see Supplemental Figure 4), indicating that similar to G121R, they are routed to lysosomes without passing through the plasma membrane. Thus T233R is transported to the plasma membrane, endocytosed, and delivered to lysosomes, whereas G121R does not transit via the cell surface en route to lysosomes.

Pharmacological chaperones rescue cell surface expression of several Cldn16 mutants. Cell-permeable chemical compounds that facilitate the folding of membrane proteins (pharmacological chaperones) have been shown to rescue surface expression of some misfolded ER-retained proteins (29). To determine whether these compounds facilitate surface transport of intracellularly retained Cldn16 mutants, their subcellular localization was monitored by immunofluorescence microscopy in cells treated with 2 commonly used pharmacological chaperones, thapsigargin and 4-phenylbutyrate (4-PBA).

Although R79L, G121R and G169R were not detected at the plasma membrane of control cells at steady state (Figure 8, A, D, and G), all 3 mutants were readily detected on the cell surface of thapsigargin-treated cells (Figure 8, B, E, and H). Surface expression of G121R and G169R was efficiently rescued by 4-PBA (Figure 8, C and F), but no effect on R79L was observed (Figure 8I). The effect of the 2 compounds on other ER-retained Cldn16 mutants was less pronounced (data not shown). Quantification showed that 3–8 times as many cells treated with the pharmacological chaperones expressed R79L, G121R, or G169R on the surface compared with control cells (Figure 8J).

To estimate the extent by which the pharmacological chaperones enhanced cellular surface expression of R79L, G121R, and G169R, we estimated surface and intracellular Cldn16 levels in treated and untreated cells. Integrated fluorescence densities of either the entire or only the intracellular cell surface area of individual, randomly selected cells labeled with anti-HA antibodies were determined, and the density associated with the cell surface was estimated from the difference of the 2 values. As shown in Figure

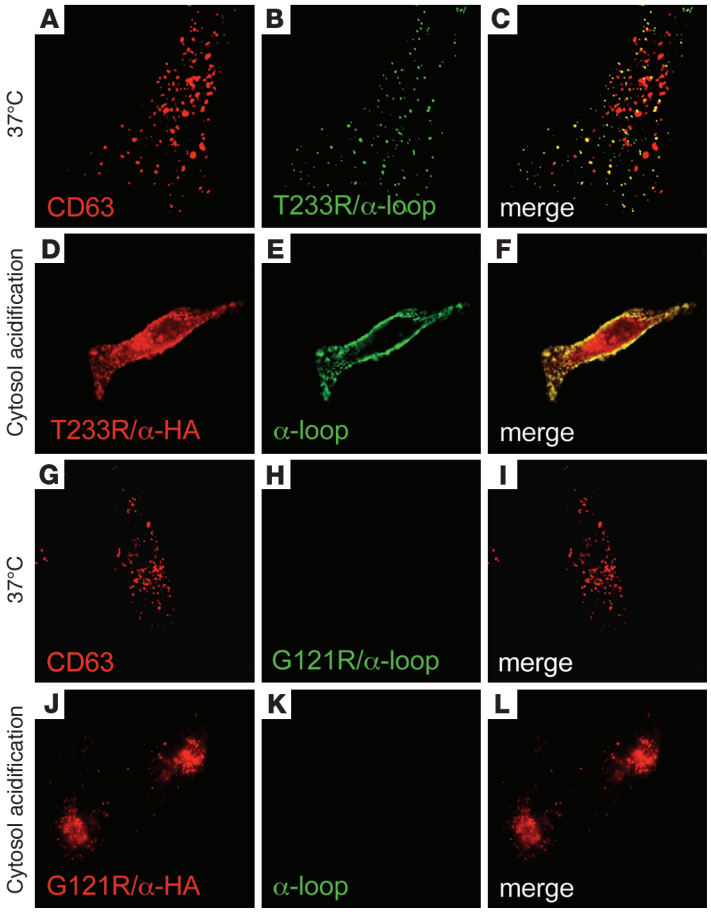

Figure 7
Cldn16 mutants that localize to lysosomes follow different pathways. Transfected HeLa cells expressing HA-tagged T233R (**A**–**F**) or G121R (**G**–**L**) were incubated in the presence of anti-loop antibodies at 37°C for 1 hour, either under normal conditions (**A**–**C** and **G**–**I**) or cytosol acidification to block endocytosis (**D**–**F** and **J**–**L**). The cells were then immunostained with antibodies to detect the anti-loop antibody (**B**, **E**, **H**, and **K**; green), the HA-tagged Cldn16 mutant (**D** and **J**; red), or the lysosomal membrane protein CD63 (**A** and **G**; red). Colocalization was apparent in the merged images (**C**, **F**, **I**, and **L**; yellow). Shown are representative images of 2–3 independent experiments.

8K, 60–70% of the total cell-associated fluorescence was present on the surface of treated cells compared with 10–25% in control cells, reflecting an estimated 2- to 6-fold increase in surface expression depending on the particular mutant and compound. Given that only the fluorescence associated with the outline of the cells was defined as surface staining, the above numbers likely underestimate the effect of the molecular chaperones.

In sum, pharmacological chaperones such as thapsigargin and 4-PBA are able to rescue cell surface expression of some intracellularly retained Cldn16 mutants, in particular R79L, G121R and G169R.

Cldn16 mutants present in TJ are defective in paracellular Mg^{2+} transport. Several Cldn16 mutants associated with FHHNC (i.e., A62V, H71D, L75P, G128A, A139T, R146T, and F162C) were delivered to the cell surface in HeLa cells (see above), suggesting that they may not localize to TJ when expressed in MDCK cells or, if present at TJs, they may be defective in paracellular Mg^{2+} transport.

To determine whether A62V, H71D, L75P, G128A, A139T, F162C, and R146T localize to TJs, MDCK cells stably expressing these mutants were generated. Consistent with the surface transport in HeLa cells and similar to WT Cldn16, these mutants were predominantly found on the cell surface of MDCK cells (data not shown). MDCK cells were grown on Transwell filters to obtain polarized cell monolayers. The different Cldn16 mutants were then analyzed for their colocalization with the TJ marker ZO-1, using confocal imaging to obtain vertical optical sections across cell monolayers. As shown in Figure 9, the different Cldn16 mutants showed colocalization with ZO-1 to a similar extent as observed for WT Cldn16, indicating that a significant fraction of these mutants is present at TJ.

The above findings indicate that the pathological phenotype associated with A62V, H71D, L75P, G128A, A138T, F162C, and R146T does not reflect a defect in cell surface expression or TJ localization. Cldn16 is thought to mediate the paracellular transport of Mg^{2+}, and patients suffering from FHHNC have impaired renal reabsorption of this divalent cation. We therefore analyzed the $P_{Mg^{2+}}$ properties of MDCK-C7 cells, a clone that develops tight monolayers characterized by a high transepithelial electrical resistance (30), expressing selected mutants using modified Ussing chambers combined with atomic absorption spectrometry (AAS). Furthermore, to explore the possibility that the rescue of cell surface expression of mutant Cldn16 may restore $P_{Mg^{2+}}$, we analyzed monolayers of cells expressing G121R or T233R following treatment with 4-PBA or inhibition of endocytosis, respectively.

$P_{Mg^{2+}}$ across monolayers of control MDCK-C7 cells and 2 clones each expressing WT Cldn16, H71D, L75P, G128A, R146T, G121R, and T233R was analyzed by AAS (Figure 10A). Basal $P_{Mg^{2+}}$ in controls was $3.9 \pm 0.2 \times 10^{-3}$ cm/h ($n = 34$, Figure 10A). Cldn16-expressing clones showed an increased $P_{M^{2+}}$ of $5.7 \pm 0.5 \times 10^{-3}$ cm/h ($n = 26$), significantly higher than control monolayers ($P < 0.05$). In contrast, none of the mutants analyzed showed an increase of $P_{Mg^{2+}}$. $P_{Mg^{2+}}$ of monolayers expressing H71D, L75P, G128A and R146T was $3.3 \pm 0.9 \times 10^{-3}$ cm/h ($n = 12$), $3.6 \pm 0.6 \times 10^{-3}$ cm/h ($n = 7$), $4.1 \pm 0.5 \times 10^{-3}$ cm/h ($n = 10$), and $3.2 \pm 0.5 \times 10^{-3}$ cm/h ($n = 12$), respectively, and in each case was not significantly different from control MDCK cells. Rescue of cell surface expression of G121R or T233R did not lead to an increase in $P_{Mg^{2+}}$, either ($2.4 \pm 0.9 \times 10^{-3}$ cm/h and $3.2 \pm 0.5 \times 10^{-3}$ cm/h, respectively; $n = 11$). Transepithelial electrical resistance (R^t) values varied between 941 ± 174 Ω cm² (T233R) and $3{,}405 \pm 303$ Ω cm² (H71D), and no correlation between $P_{Mg^{2+}}$ and R^t was observed (Figure 10B). Analysis of sodium permeability/chloride permeability ratios (P_{Na}/P_{Cl} ratios) was performed by measuring dilution potential changes after replacing 59.5 mM NaCl with 119 mM mannitol ($n = 11$–12). P_{Na}/P_{Cl} ratios were not significantly altered by the expression of WT Cldn16, H71D, G126A, or R146T (Figure 10C).

These data show that at least 4 of the Cldn16 mutants linked to FHHNC that are correctly incorporated into TJ are defective in mediating paracellular $P_{Mg^{2+}}$. Rescuing surface expression of 2 mutants failed to increase $P_{Mg^{2+}}$.

Discussion

Although more than 20 mutations in Cldn16 have been described in patients suffering from FHHNC (2–4), little is known about the

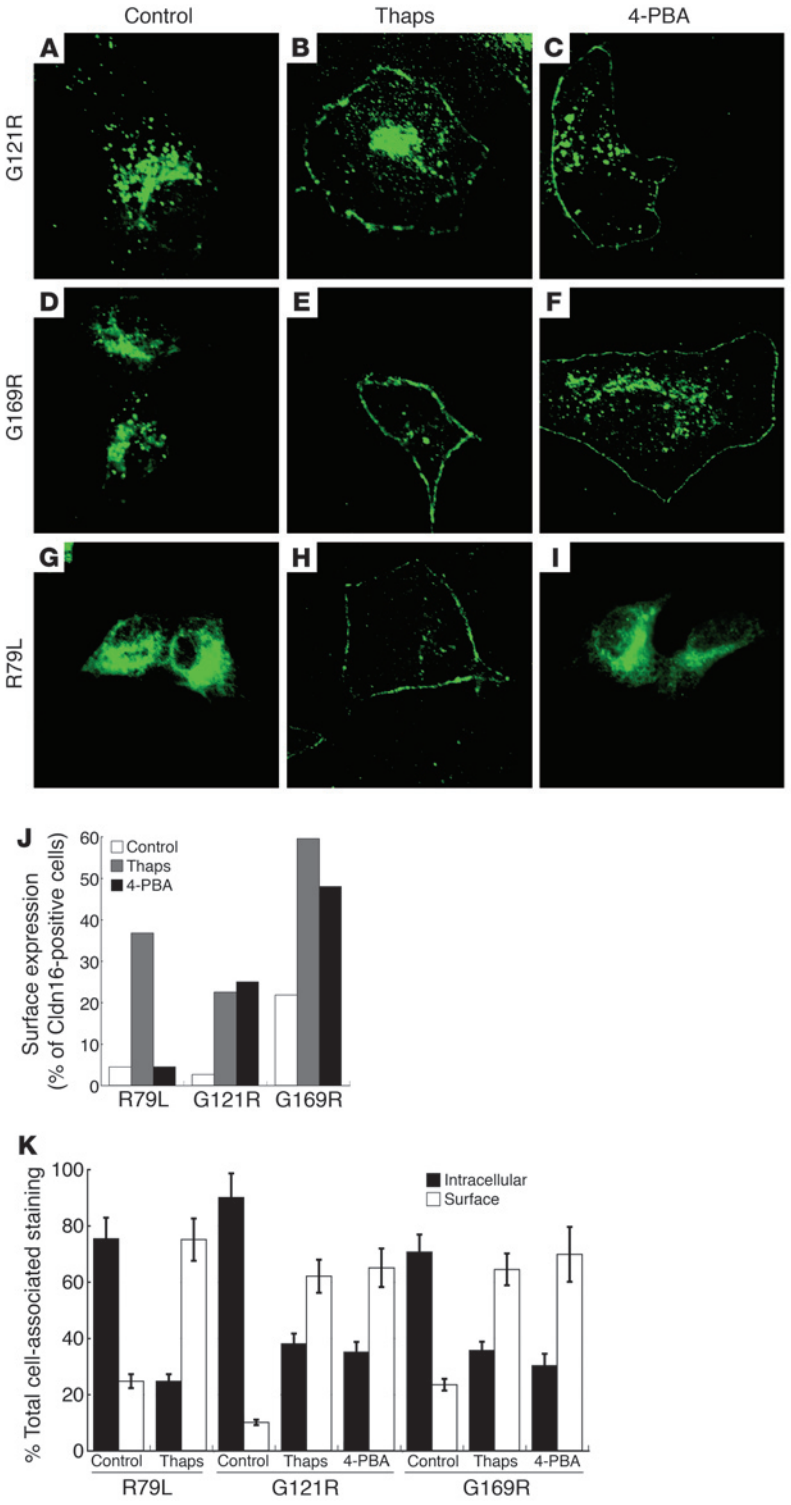

Figure 8
Chemical chaperones rescue cell surface expression of several Cldn16 mutants. Transfected HeLa cells expressing HA-tagged G121R (**A**–**C**), G169R (**D**–**F**), or R79L (**G**–**I**) were incubated in the presence of vehicle (Control; **A**, **D**, and **G**), thapsigargin (Thaps; **B**, **E**, and **H**) or 4-PBA (**C**, **F**, and **I**). The cells were then immunostained with antibodies to detect the Cldn16 mutant (green). Shown are representative images of 2–3 independent experiments. (**J**) Quantification of the number of cells that expressed mutant Cldn16 on the cell surface in response to thapsigargin or 4-PBA. One hundred randomly chosen cells expressing the Cldn16 mutant were analyzed, and the fraction of cells showing surface expression in the presence of the pharmacological chaperones was determined. Data from 3 independent experiments is shown. (**K**) Quantification of the fraction of total cell-associated mutant Cldn16 present on the surface of individual cells in response to thapsigargin or 4-PBA. Integrated fluorescence densities of either the entire or only the intracellular cell surface area of 50–60 individual, randomly selected cells labeled with anti-HA antibodies were determined. The density associated with the cell surface was estimated from the difference of the 2 values and normalized to total cell-associated staining. Given that only the fluorescence associated with the outline of the cells was defined as surface staining, these results likely underestimate the effect of the molecular chaperones.

molecular mechanism by which these mutations affect Cldn16 function. Given that FHHNC is characterized by the failure of the kidney to reabsorb filtered Mg^{2+} and Ca^{2+} (2–4) and Cldn16 facilitates paracellular divalent cation transport (31), it has been suggested that the mutations associated with FHHNC interfere with the ability of Cldn16 to transport Mg^{2+} (4). The clinical course of FHHNC is highly variable, and no apparent genotype-phenotype correlation has been observed among patients with the same type of mutation, although a close intrafamilial concordance was found with respect to development of renal failure (2, 32). The variable clinical progression of the disease and the recent report that a mutation in the cytosolic tail results in lysosomal mistargeting of Cldn16 (11) indicate that mutations linked to FHHNC may affect more than paracellular divalent cation transport function. Indeed, the present systematic analysis of most of the Cldn16 mutations linked to FHHNC described to date revealed defects in either intracellular trafficking of Cldn16 or its function in paracellular Mg^{2+} transport.

During biosynthesis and insertion into the ER, integral membrane proteins associate with chaperones that facilitate their folding and retain them in the ER until they have attained their correct conformation (33). In the event that a newly synthesized protein does not fold properly, it is removed from the ER, ubiquitinated, and degraded by the proteasome (34). This quality-control mechanism ensures that only correctly folded and functional proteins exit the ER for delivery to their final destination. While WT Cldn16 is readily transported to the plasma membrane, several Cldn16 mutants (i.e., W47X, N53fs, G92V, L97P, G163D, S165F, and S165P) were detected in the ER and absent from the plasma membrane. These mutants were retained in the ER since they did not reach the Golgi complex at 20°C, conditions which allow the transfer of proteins from the ER to the Golgi complex but block transport within and beyond the Golgi complex and the TGN (24, 25). This behavior is similar to the cystic fibrosis transmembrane conductance regulator (CFTR) mutant

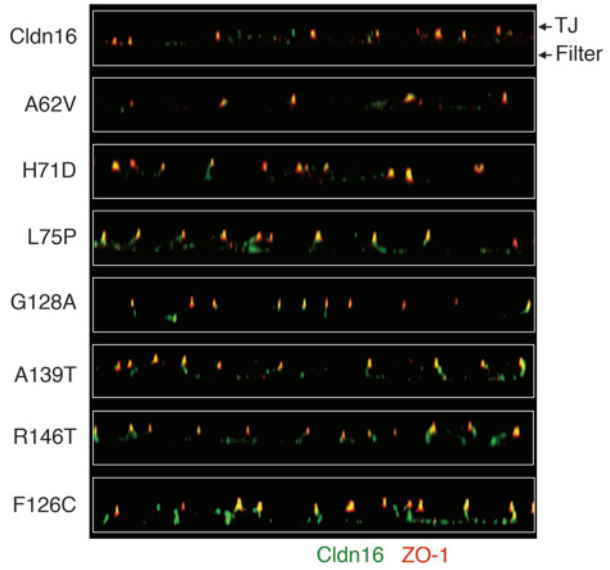

Figure 9
TJ localization of Cldn16 mutants expressed on the cell surface. Transfected MDCK cells expressing Cldn16 mutants that are delivered to the cell surface were grown on permeable polycarbonate filters to obtain polarized cell monolayers. The cells were then fixed, permeabilized, and stained with antibodies to HA to detect the Cldn16 mutants (green) or the TJ marker ZO-1 (red). Shown are representative images of 2–3 independent experiments.

CFTRΔF508, the most common mutation in patients suffering from cystic fibrosis, which also fails to leave the ER at lower temperatures (35). Cells expressing Cldn16 mutants that are retained in the ER showed increased staining for ubiquitin, which extensively colocalized with the mutant Cldn16 and was further enhanced when cells were treated with a proteasome inhibitor. Furthermore, inhibition of proteasomal activity led to the intracellular accumulation of the ER-retained Cldn16 mutants and slowed their turnover rate. These data indicate that W47X, N53fs, G92V, L97P, G121R, G163D, S165F, and S165P are probably defective in folding, membrane topology, and/or oligomerization and are therefore recognized by the ER quality-control machinery and tagged for destruction. Mutations in integral membrane proteins that result in ER retention have been classified into those that are degraded (class I) and those that interfere with degradation and result in ER accumulation (class II) (36). According to this classification, the ER-retained Cldn16 mutants belong to the class I type, which is less likely to trigger chronic pathological ER stress signals (36, 37). In a recent study, R79L and S165P were also localized to the ER in LLC-PK1 cells, whereas L97P and G163D could not be expressed in LLC-PK1 cells (12).

Three of the Cldn16 mutants analyzed (i.e., L81F, L81W, and R79X) were competent to exit the ER and predominantly localize to the Golgi complex at steady state. Cells expressing these mutants failed to bind or internalize the anti-loop antibodies, which indicates that these mutants do not reach the cell surface. These mutants accumulate in the Golgi complex at 20°C, and release from the 20°C block results in their detection in lysosomes, indicating that if accumulated in the Golgi beyond a particular threshold, they may be delivered to lysosomes. The exit of these mutants may be blocked or slowed as part of a quality-control system operating in the Golgi complex or the TGN (38).

T233R and G121R showed predominant lysosomal localization even at steady state, suggesting efficient transport out of the Golgi complex. T233R was able to bind and internalize anti-loop antibodies at 37°C and accumulated at the cell surface when endocytosis was inhibited, showing that a significant fraction of this mutant transits via the plasma membrane and then reaches lysosomes following endocytosis. In contrast, G121R did not appear to be routed via the cell surface and is probably delivered from the Golgi complex to lysosomes either directly or via endosomes. How the G121R mutation facilitates direct transport of G121R to lysosomes is not clear. G121 is located in proximity of the cytosolic face of the third transmembrane domain, and the preceding cytosolic loop contains a tyrosine-containing sequence (YIKV) reminiscent of lysosomal targeting signals. The G121R substitution may induce a conformational change that exposes and facilitates the recognition of this motif by the TGN-sorting machinery. L81F and G121R have recently also been localized to TJs in LLC-PK1 cells (12), and although we failed to detect surface delivery of G121R in HeLa or MDCK cells, plasma membrane expression of this mutant could be rescued by 4-PBA or thapsigargin.

The remaining mutants we analyzed (i.e., A62V, H71D, L75P, G128A, A139T, R146T, and F162C) were delivered to the cell surface, where, similar to WT Cldn16, they extensively colocalized with the TJ marker ZO-1. L75P, A139T, and F162C were found in TJs of LLC-PK1 cells, whereas R146T and G128A could not be expressed in these cells (12). To explore a direct effect of point mutations in Cldn16 on $P_{Mg^{2+}}$, monolayers of stably transfected MDCK-C7 cells were used for Mg^{2+} flux analyses. AAS emerged as a suitable technique for direct measurement of $P_{Mg^{2+}}$. Expression of Cldn16 resulted in an increased $P_{Mg^{2+}}$ of cell monolayers, in agreement with a recent study in LLC-PK1 cells, where permeability was calculated from dilution potentials (12). Compared with LLC-PK1 cells, overexpression of Cldn16 in MDCK cells resulted in a 6-fold lower $P_{Mg^{2+}}$ ($5.7 \pm 0.5 \times 10^{-3}$ cm/h versus $10.7 \pm 0.06 \times 10^{-6}$ cm/s, equivalent to 38.7×10^{-3} cm/h) and did not alter the permeability for Na^+. This phenomenon, also observed by Hou et al. for MDCK II cells (12), may reflect differences in the endogenous R^t and TJ protein expression pattern in the different epithelial cell lines used in these studies. Differences in the composition and expression levels of endogenous claudins, in particular, are likely to differentially modulate exogenous Cldn16 function (39, 40). Furthermore, differences between MDCK and LLC-PK1 cells with respect to polarized trafficking and localization of endogenous membrane proteins are well established (41). In contrast to WT Cldn16, expression of H71D, L75P, G128A, and R146T did not lead to increased Mg^{2+} flux compared with control cells, providing evidence for the inactivation of paracellular Mg^{2+} transport in vitro by point mutations in Cldn16 linked to FHHNC. In LLC-PK1 cells, G128A and R146T were not expressed, and the function of A139T and F162C (which we did not analyze in the present study) was impaired and unaffected, respectively (12). The extracellular loops of Cldn16 are rich in charged amino acids, negatively charged residues thought to be of particular importance for the paracellular transport of divalent cations (4, 12). Interestingly, however, the mutations found so far in patients with FHHNC do not affect negatively charged amino acids. Therefore, these mutations may alter the secondary or tertiary structure of Cldn16 and hence impede paracellular Mg^{2+} transport. For example, the H71D substitution may disrupt electrostatic interactions, the L75P mutation may alter protein conformation, and F162C may generate aberrant

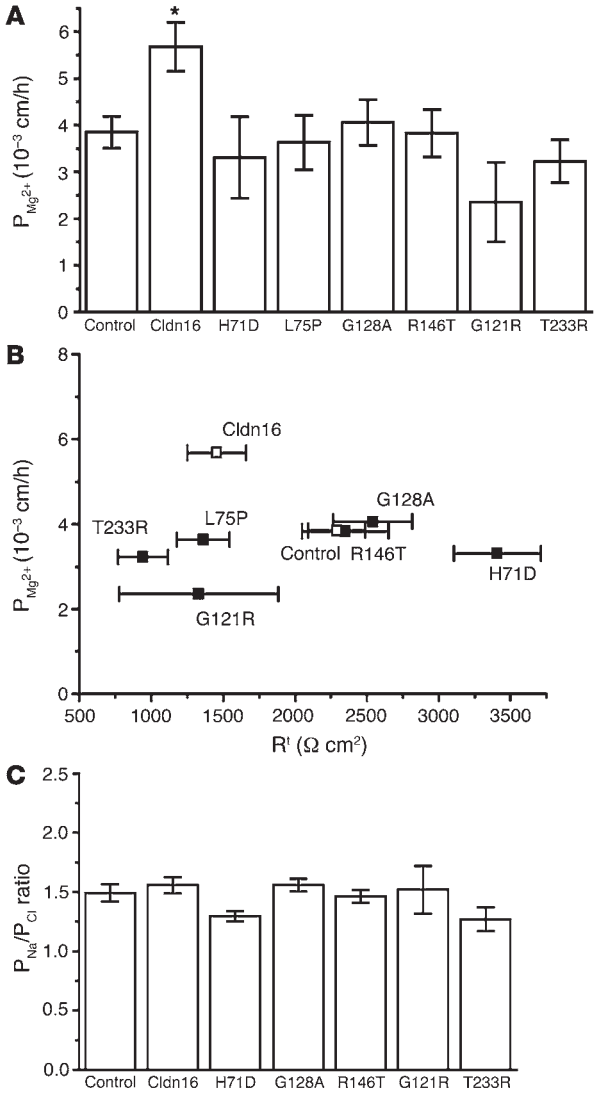

Figure 10

Measurements of $P_{Mg^{2+}}$, R^t, and P_{Na}/P_{Cl} ratios. (**A**) $P_{Mg^{2+}}$. Monolayers of stable transfected MDCK-C7 cells were grown on permeable supports and mounted in Ussing chambers. Mg^{2+} was added to the basolateral side, and net flux was measured by means of AAS. *$P < 0.05$ versus control. (**B**) Comparison of R^t to $P_{Mg^{2+}}$. R^t of the clones ranged between 941 ± 174 Ω cm² (T233R) and 3,406 ± 303 Ω cm² (H71D). No correlation of $P_{Mg^{2+}}$ and R^t was observed (n = 7–16). (**C**) P_{Na}/P_{Cl} ratios. Dilution potentials were measured with modified Ringer's solution on the luminal or serosal side, and the data from the 2 conditions was pooled (n = 6 per group). No significant changes were observed in cells expressing WT Cldn16 or the mutants indicated.

disulfide bonds. Little is known about the structural requirements for oligomerization, either in *cis* or in *trans*, of Cldn16, which may also be affected by some of these mutations.

Interestingly, Cldn16 can internalize via a clathrin-mediated pathway. Similar to WT Cldn16, mutants transported to the cell surface were detected in small vesicles positive for the early endosome marker EEA1. Since Cldn16 was also present in early endosomes in the absence of anti-loop antibodies, internalization was not induced by antibody cross-linking. Cldn16 encodes several putative internalization signals within the cytosolic loop (YIKV) and the C-terminal tail (YRLS, YSAA, YSAP, and YAVD), which could mediate clathrin-dependent endocytosis by interacting with the clathirn adaptor protein-2. Although endocytosis of endogenous Cldn16 was detected in MDCK cells, a larger fraction was present in endosomes of HeLa cells, possibly because in MDCK cells Cldn16 is more efficiently retained at the surface through its interaction with ZO-1. This interpretation is consistent with the observation that the association between Cldn16 and ZO-1 increases the reabsorption of divalent cations in renal epithelial cells (31). Indeed T233R, which no longer interacts with ZO-1, was efficiently internalized, indicating that it may be retained less effectively at TJ than WT Cldn16 and, as a consequence, be subject to a faster rate of lysosomal delivery. Alternatively, the T233R mutation could affect postendocytic sorting by diverting the protein from a recycling into a lysosomal pathway, or ZO-1 bound to Cldn16 could prevent lysosomal delivery. Indeed the ability of connexins to associate with ZO-1 has been correlated with a longer half-life of these gap junction proteins (42, 43).

A clear correlation between the location of a particular mutation and its effect on Cldn16 localization could not be established, although mutations occurring near to each other generally showed a similar defect. For example, mutations in the N-terminal half of the first extracellular loop (i.e., W47X and N53fs), the first transmembrane domain (i.e., L75P and G92V), or the C-terminal region of the second extracellular loop (i.e., G163D, S165P, and S165F) led to ER retention, whereas mutations affecting the C terminus of the first extracellular loop (i.e., R79L and L81F) resulted in Golgi localization. In addition, several mutations that lead to different substitutions of the same amino acid (i.e., R79P/L, L81W/F, and S165P/F) displayed similar localization. Furthermore, there was no apparent correlation between a particular mutation or its subcellular localization and a clinical phenotype. More than 20 different mutations in *Cldn16* have been reported to date (1–4, 11, 32, 44). Of the 15 individuals carrying the L81F mutation, 11 were homozygous for the mutation and the remainder were compound heterozygotes (44). Individuals homozygous for this locus lacked a phenotype-genotype correlation, and at the conclusion of the study, 5 individuals had a glomerular filtration rate (GFR) greater than 60 ml/min/1.73 m² body surface area, another 5 individuals had a GFR below 60 ml/min/1.73 m² body surface area, 1 patient was on dialysis, and 1 had undergone renal transplantation. There was no linear correlation between disease progression and age. Patients with the L75P mutation were all compound heterozygous carriers with various other mutations on the second allele. Renal function ranged from being unaffected to end-stage renal failure and renal transplantation. So far only 2 mutations, W47X/L81F and T233R, have shown a consistent clinical phenotype among different patients. Two patients from the same family carrying W47X/L81F needed renal replacement therapy (44), whereas 4 patients from 2 different families with the T233R mutation presented a GFR greater than 80 ml/min/m² body surface area (11). However, the collective in each case was too small for a definite phenotype-genotype analysis, and more patients will have to be identified to verify this tendency.

Intriguingly, pharmacological chaperones such as thapsigargin or 4-PBA were able to rescue cell surface transport of some intracellularly retained Cldn16 mutants, in particular R79L,

G121R, and G169R. The 2 compounds not only increased the fraction of cells showing surface expression of the mutant proteins, but also increased the fraction of the mutant protein that was present on the surface of individual cells. The exact mechanisms by which exogenous chaperones function are not fully understood and differ from one compound to the other, but they may stabilize misfolded proteins, prevent their aggregation or nonproductive interaction with ER resident proteins, or affect the activity of chaperones, thus allowing the retained protein to exit the ER (reviewed in ref. 29). Stabilizing compounds such as glycerol or DMSO have been used to rescue conformationally defective mutants of the CFTR (45), aquaporin-2 (46), and the V2 vasopressin receptor (47). The compound 4-PBA, which reduces mRNA and protein levels of the heat-shock protein Hsc70 (48, 49), and thapsigargin, which depletes ER calcium stores (50), rescue ER-retained mutants of the CFTR and K^+ channels, respectively (48, 49, 51, 52). In particular, 4-PBA shows low cytotoxicity and is in clinical trials for cystic fibrosis (53, 54). Thapsigargin and 4-PBA showed a dramatic increase in the surface expression of G121R and G169R. Thapsigargin, in addition, rescued surface expression of R79L. Since the effectiveness of pharmacological chaperones likely depends on the severity of the conformational defect (29), G169R, R79L, and G121R may be less severely misfolded than the other ER-retained Cldn16 mutants. In addition to pharmaceutical chaperones, endocytosis inhibitors may provide a therapeutic means of increasing the amount of Cldn16 present on the cell surface in patients carrying T233R or mutations with a similar defect. These findings may open new therapeutic avenues for patients suffering from FHHNC. However, rescuing cell surface expression of 2 mutants, G121R and T233R, did not restore the increase in Mg^{2+} observed for WT Cldn16. At least for G121R, the protein may not be functional as observed in LLC-PK1 cells, where this mutant is present in TJs (12). For the other mutants, either insufficient protein may be present on the cell surface or the mutant protein may not localize to TJs or, in the case of T233R, may require binding to ZO-1 for function. Given the mild phenotype in patients carrying the T233R mutation (11), it will be of interest to determine in mouse models to what extent this and other mutations rescue Cldn16 function under different experimental conditions.

In conclusion, mutations in Cldn16 associated with FHHNC can be classified into 2 groups: (a) mutations that affect intracellular trafficking of Cldn16 and result in either ER retention, Golgi accumulation, or lysosomal mistargeting; and (b) those that do not interfere with surface expression or TJ localization of Cldn16 but abolish its ability to facilitate paracellular divalent cation transport. The benefits of therapeutic intervention in FHHNC are only symptomatic, and most patients eventually require kidney replacement therapy (1). Characterizing the molecular defects of Cldn16 mutants associated with FHHNC may open new venues for therapeutic intervention.

Methods

Antibodies and chemicals. Rabbit anti–ZO-1 (Zymed), GM130, and EEA1 (BD Biosciences — Pharmingen), calreticulin (ABR), rat monoclonal anti-HA (Roche Diagnostic Corp.), and mouse monoclonal anti-CD63 (Developmental Studies Hybridoma Bank), ubiquitin (Santa Cruz Biotechnology Inc.), and EEA1 (BD Biosciences — Pharmingen) antibodies were used. A rabbit polyclonal anti-loop antibody to the first extracellular loop of Cldn16 (amino acids 52–66) was raised (BioGenes). Unless otherwise noted, all chemicals were from Sigma-Aldrich. Stock solutions of ALLN (26 mM in DMSO; Calbiochem), cycloheximide (2 mg/ml in H_2O), sodium 4-PBA (100 mM in H_2O; Calbiochem), and thapsigargin (100 μM in H_2O; A.G. Scientific Inc.) were stored at –20°C.

Plasmids and cDNAs. The isolation of a full-length human Cldn16 cDNA and the addition of an N-terminal HA tag have been described previously (11). Mutations in Cldn16 linked to FHHNC were introduced by PCR using suitable overlapping primers, cloned into the pcDNA3 expression vector (Invitrogen Corp.), and all constructs were verified by sequencing.

Cell culture and transfection. MDCK II, MDCK-C7 (30), 293T, and HeLa cells were cultured and stably or transiently transfected with the different Cldn16 cDNAs as described previously (11, 55, 56) to obtain similar expression levels. Cells were used for experiments 24 hours after transient transfection.

Immunofluorescence labeling. Cells were grown on coverslips or Transwell polycarbonate filter units and processed for confocal immunofluorescence microscopy as described previously (11, 20, 55, 56) using antibodies to HA (1:100 dilution), calreticulin (1:300 dilution), GM130 (1:100 dilution), CD63 (1:300 dilution), Lamp2 (1:100 dilution), EEA1 (1:100 dilution), or ubiquitin (1:100 dilution) and suitable fluorescently labeled secondary antibodies (Invitrogen Corp.).

Monitoring of cell surface expression and endocytosis. Transiently transfected HeLa or MDCK cells were incubated with the anti-loop antibody (1:100 dilution) for 1 hour at 37°C. The cells were then washed in ice-cold PBS containing 0.9 mM $CaCl_2$ and 0.5 mM $MgCl_2$, fixed, permeabilized, and stained with labeled secondary antibodies. For competitions, the anti-loop antibody was preincubated in the presence of a 100-μM molar excess of the peptide used for immunization. To estimate the amount of total cell-associated Cldn16 present on the surface of individual cells in response to thapsigargin or 4-PBA treatment, integrated fluorescence densities either of the entire or of only the intracellular cell surface area of individual, randomly selected cells labeled with anti-HA antibodies were determined using nonconfocal imaging. The density associated with the cell surface was then estimated from the difference of the 2 values and normalized to total cell-associated labeling.

Temperature blocks, inhibition of protein synthesis and endocytosis, and use of pharmacological chaperones. Transiently transfected HeLa cells were incubated for 3 hours at 20°C to accumulate proteins in the Golgi complex (24). The cells were then either fixed or transferred to 37°C in the presence of 20 μg/ml cycloheximide and 100 μM ALLN for 1 or 6 hours. The role of clathrin in Cldn16 internalization was analyzed by incubating transiently transfected HeLa cells for 1 hour in the presence of anti-loop antibody in RPMI supplemented with 0.4 M sucrose (hypotonic conditions) or 20 mM 2-[N-morpholino]ethanesulfonic acid and succinic acid (pH 5.5) (cytosol acidification). To block caveolae-mediated uptake, 2 U/ml cholesterol oxidase was added to the media in the presence of anti-loop antibody. Thapsigargin (1 μM) and 4-PBA (1 mM) were added to transfected HeLa cells in RPMI culture media for 3 and 24–48 hours, respectively, at 37°C, and anti-loop antibodies were added to the media for the last hour of the incubation. After the respective treatments, cells were washed and processed for immunofluorescence microscopy as described above.

Western blot analysis and immunoprecipitation. Transiently transfected 293T cells were incubated for different times with the proteasomal inhibitor ALLN (100 μM) in the absence or presence of cycloheximide (20 μg/ml) and harvested. The protein concentration of extracts was determined using Bradford assays, and 50–100 μg of protein lysate was analyzed by SDS-PAGE and Western blot (11, 55, 56) using antibodies to HA (1:1,000 dilution) and actin (1:2,500 dilution).

Measurement of $P_{Mg^{2+}}$. Stably transfected MDCK-C7 clones were grown on porous polycarbonate inserts (0.6 cm^2 effective area, Millicell-HA; Millipore). On day 7, inserts were mounted in Ussing chambers, and water-jacketed gas lifts were filled with 10 ml circulating Ringer's solu-

tion [119 mM NaCl, 21 mM $NaHCO_3$, 5.4 mM KCl, 1.2 mM $CaCl_2$, 3 mM HEPES, 10 mM D(+)-glucose] on each side. The Ringer's solution was adjusted to pH 7.8 with NaOH and gassed with 95% O_2 and 5% CO_2 to ensure a pH value of 7.4 during the experiments at 37°C. Measurement of unidirectional fluxes from the basolateral to the apical side was performed under short-circuit conditions with $MgSO_4$. Four 30-minute flux periods were analyzed (57). Upon initiation, a 1-ml sample was taken from the donor (apical) side, and $MgSO_4^{2+}$ (10 mM) was added to the basolateral side. Mg^{2+} fluxes were analyzed by flame AAS. Samples were mixed with H_2O containing 0.1% La_2O_3 and 0.16% HCl. Lanthanum oxide was added to suppress phosphate interferences with the ionization of calcium and magnesium in the AAS flame and HCl for proper pH adjustment (pH 2). The atomic absorption of magnesium was measured in an oxidizing air-acetylene flame at 285.2 nm. The measurements were calibrated with solutions of 0.025, 0.075, 0.1, 0.3, and 0.5 μg/ml Mg^{2+} in H_2O containing 0.1% La_2O_3 and 0.16% HCl. $P_{Mg^{2+}}$ was calculated from resulting fluxes ($P_{Mg^{2+}}$ = flux/concentration). Results showed the suitability of the method for direct measurement of magnesium in unidirectional flux experiments.

P_{Na}/P_{Cl} ratio measurements. Dilution potentials were measured with modified Ringer's solution on the mucosal or serosal side, and the data from both conditions were pooled. In the modified Ringer's solution, 59.5 mM NaCl was replaced by 119 mM mannitol. Standard Ringer's solution contained 119 mM NaCl, 21 mM $NaHCO_3$, 5.4 mM KCl, 1 mM $MgSO_4$, 1.2 mM $CaCl_2$, 3 mM HEPES, and 10 mM glucose. Low-Na^+ Ringer's solution contained no NaCl, 21 mM $NaHCO_3$, 5.4 mM KCl, 1 mM $MgSO_4$, 1.2 mM $CaCl_2$, 3 mM HEPES, 10 mM glucose, and 238 mM mannitol. During the experiment, 50% of standard Ringer's solution was substituted with low-Na^+ Ringer's solution. Junction potentials were taken into account.

Statistical analysis. Where applicable, data are expressed as the mean ± SEM. Statistical analysis was performed using 2-tailed Student's *t* test. Values of $P < 0.05$ were considered statistically significant.

Note added in proof. We recently identified a novel Cldn16 mutant, L203X, which lacks most of the C-terminal cytosolic domain and displays intracellular trafficking defects (58).

Acknowledgments

We thank Anja Fromm and Brigitte Papanis for excellent technical assistance. MDCK-C7 cells were a gift from Hans Oberleitner (University of Münster, Münster, Germany). This work was supported by the Agency for Science, Technology and Research, Singapore (A*STAR) and the Deutsche Forschungsgemeinschaft (DFG Fr 652/4). W. Hunziker is an adjunct faculty member at the Department of Physiology, National University of Singapore. D. Müller is a member of the European Renal Genome Project (EuReGene) Consortium (6th Framework Programme of the European Union, FP6005085).

Received for publication July 19, 2005, and accepted in revised form January 10, 2006.

Address correspondence to: Walter Hunziker, Epithelial Cell Biology Laboratory, Institute of Molecular and Cell Biology, 61 Biopolis Drive, 138673 Singapore. Phone: 65-6586-9599; Fax: 65-6779-1117; E-mail: hunziker@imcb.a-star.edu.sg.

P. Jaya Kausalya and Salah Amasheh contributed equally to this work.

1. Asplin, J.R., Favus, M.J., and Coe, F.L. 1996. Nephrolithiasis. In *The kidney*. 5th edition. B.M. Brenner, editor. W.B. Saunders. Philadelphia, Pennsylvania, USA. 1893–1935.
2. Weber, S., et al. 2000. Familial hypomagnesemia with hypercalciuria and nephrocalcinosis maps to chromosome 3q27 and is associated with mutations in the PCLN-1 gene. *Eur. J. Hum. Genet.* **8**:414–422.
3. Blanchard, A., et al. 2001. Paracellin-1 is critical for magnesium and calcium reabsorption in the human thick ascending limb of Henle. *Kidney Int.* **59**:2206–2215.
4. Simon, D.B., et al. 1999. Paracellin-1, a renal tight junction protein required for paracellular Mg^{2+} resorption. *Science.* **285**:103–106.
5. Weber, S., et al. 2001. Primary gene structure and expression studies of rodent paracellin-1. *J. Am. Soc. Nephrol.* **12**:2664–2672.
6. Loh, Y., Christoffels, A., Brenner, S., Hunziker, W., and Venkatesh, B. 2004. Extensive expansion of the claudin gene family in the teleost fish, Fugu rubripes. *Genome Res.* **14**:1248–1257.
7. Turksen, K., and Troy, T.C. 2004. Barriers built on claudins. *J. Cell Sci.* **117**:2435–2447.
8. Furuse, M., Sasaki, H., and Tsukita, S. 1999. Manner of interaction of heterogeneous claudin species within and between tight junction strands. *J. Cell Biol.* **147**:891–903.
9. Anderson, J.M., Van Itallie, C.M., and Fanning, A.S. 2004. Setting up a selective barrier at the apical junction complex. *Curr. Opin. Cell Biol.* **16**:140–145.
10. Van Itallie, C.M., and Anderson, J.M. 2004. The molecular physiology of tight junction pores. *Physiology (Bethesda).* **19**:331–338.
11. Müller, D., et al. 2003. A novel claudin 16 mutation associated with childhood hypercalciuria abolishes binding to ZO-1 and results in lysosomal mistargeting. *Am. J. Hum. Genet.* **73**:1293–1301.
12. Hou, J., Paul, D.L., and Goodenough, D.A. 2005. Paracellin-1 and the modulation of ion selectivity of tight junctions. *J. Cell Sci.* **118**:5109–5118.
13. Damke, H., Baba, T., Warnock, D.E., and Schmid, S.L. 1994. Induction of mutant dynamin specifically blocks endocytic coated vesicle formation. *J. Cell Biol.* **127**:915–934.
14. Henley, J.R., Cao, H., and McNiven, M.A. 1999. Participation of dynamin in the biogenesis of cytoplasmic vesicles. *FASEB J.* **13**(Suppl. 2):S243–S247.
15. Henley, J.R., Krueger, E.W., Oswald, B.J., and McNiven, M.A. 1998. Dynamin-mediated internalization of caveolae. *J. Cell Biol.* **141**:85–99.
16. Sandvig, K., Olsnes, S., Petersen, O.W., and van Deurs, B. 1987. Acidification of the cytosol inhibits endocytosis from coated pits. *J. Cell Biol.* **105**:679–689.
17. Heuser, J.E., and Anderson, R.G. 1989. Hypertonic media inhibit receptor-mediated endocytosis by blocking clathrin-coated pit formation. *J. Cell Biol.* **108**:389–400.
18. Smart, E.J., Ying, Y.S., Conrad, P.A., and Anderson, R.G. 1994. Caveolin moves from caveolae to the Golgi apparatus in response to cholesterol oxidation. *J. Cell Biol.* **127**:1185–1197.
19. Coconnier, M.H., Lorrot, M., Barbat, A., Laboisse, C., and Servin, A.L. 2000. Listeriolysin O-induced stimulation of mucin exocytosis in polarized intestinal mucin-secreting cells: evidence for toxin recognition of membrane-associated lipids and subsequent toxin internalization through caveolae. *Cell. Microbiol.* **2**:487–504.
20. Honing, S., and Hunziker, W. 1995. Cytoplasmic determinants involved in direct lysosomal sorting, endocytosis, and basolateral targeting of rat lgp120 (lamp-I) in MDCK cells. *J. Cell Biol.* **128**:321–332.
21. Sonnichsen, B., et al. 1994. Retention and retrieval: both mechanisms cooperate to maintain calreticulin in the endoplasmic reticulum. *J. Cell Sci.* **107**:2705–2717.
22. Nakamura, N., et al. 1995. Characterization of a cis-Golgi matrix protein, GM130. *J. Cell Biol.* **131**:1715–1726.
23. Metzelaar, M.J., et al. 1991. CD63 antigen. A novel lysosomal membrane glycoprotein, cloned by a screening procedure for intracellular antigens in eukaryotic cells. *J. Biol. Chem.* **266**:3239–3245.
24. VanSlyke, J.K., Deschenes, S.M., and Musil, L.S. 2000. Intracellular transport, assembly, and degradation of wild-type and disease-linked mutant gap junction proteins. *Mol. Biol. Cell.* **11**:1933–1946.
25. Matlin, K.S., and Simons, K. 1983. Reduced temperature prevents transfer of a membrane glycoprotein to the cell surface but does not prevent terminal glycosylation. *Cell.* **34**:233–243.
26. Rock, K.L., et al. 1994. Inhibitors of the proteasome block the degradation of most cell proteins and the generation of peptides presented on MHC class I molecules. *Cell.* **78**:761–771.
27. Wettstein, F.O., Noll, H., and Penman, S. 1964. Effect of cycloheximide on ribosomal aggregates engaged in protein synthesis in vitro. *Biochim. Biophys. Acta.* **87**:525–528.
28. Hunziker, W., and Geuze, H.J. 1996. Intracellular trafficking of lysosomal membrane proteins. *Bioessays.* **18**:379–389.
29. Ulloa-Aguirre, A., Janovick, J.A., Brothers, S.P., and Conn, P.M. 2004. Pharmacologic rescue of conformationally-defective proteins: implications for the treatment of human disease. *Traffic.* **5**:821–837.
30. Amasheh, S., et al. 2002. Claudin-2 expression induces cation-selective channels in tight junctions of epithelial cells. *J. Cell Sci.* **115**:4969–4976.
31. Ikari, A., et al. 2004. Association of paracellin-1 with ZO-1 augments the reabsorption of divalent cations in renal epithelial cells. *J. Biol. Chem.* **279**:54826–54832.
32. Wolf, M.T., Dotsch, J., Konrad, M., Boswald, M., and Rascher, W. 2002. Follow-up of five patients

with FHHNC due to mutations in the Paracellin-1 gene. *Pediatr. Nephrol.* **17**:602–608.
33. Sitia, R., and Braakman, I. 2003. Quality control in the endoplasmic reticulum protein factory. *Nature.* **426**:891–894.
34. Jarosch, E., Geiss-Friedlander, R., Meusser, B., Walter, J., and Sommer, T. 2002. Protein dislocation from the endoplasmic reticulum--pulling out the suspect. *Traffic.* **3**:530–536.
35. Denning, G.M., et al. 1992. Processing of mutant cystic fibrosis transmembrane conductance regulator is temperature-sensitive. *Nature.* **358**:761–764.
36. Aridor, M., and Balch, W.E. 1999. Integration of endoplasmic reticulum signaling in health and disease. *Nat. Med.* **5**:745–751.
37. Johnston, J.A., Ward, C.L., and Kopito, R.R. 1998. Aggresomes: a cellular response to misfolded proteins. *J. Cell Biol.* **143**:1883–1898.
38. Arvan, P., Zhao, X., Ramos-Castaneda, J., and Chang, A. 2002. Secretory pathway quality control operating in Golgi, plasmalemmal, and endosomal systems. *Traffic.* **3**:771–780.
39. Tang, V.W., and Goodenough, D.A. 2003. Paracellular ion channel at the tight junction. *Biophys. J.* **84**:1660–1673.
40. Van Itallie, C.M., and Anderson, J.M. 2005. Claudins and epithelial paracellular transport. *Annu. Rev. Physiol.* doi:10.1146/annurev.physiol.68.040104.131404.
41. Folsch, H., Ohno, H., Bonifacino, J.S., and Mellman, I. 1999. A novel clathrin adaptor complex mediates basolateral targeting in polarized epithelial cells. *Cell.* **99**:189–198.
42. Barker, R.J., Price, R.L., and Gourdie, R.G. 2001. Increased co-localization of connexin43 and ZO-1 in dissociated adult myocytes. *Cell Commun. Adhes.* **8**:205–208.
43. Toyofuku, T., et al. 2001. c-Src regulates the interaction between connexin-43 and ZO-1 in cardiac myocytes. *J. Biol. Chem.* **276**:1780–1788.
44. Weber, S., et al. 2001. Novel paracellin-1 mutations in 25 families with familial hypomagnesemia with hypercalciuria and nephrocalcinosis. *J. Am. Soc. Nephrol.* **12**:1872–1881.
45. Sato, S., Ward, C.L., Krouse, M.E., Wine, J.J., and Kopito, R.R. 1996. Glycerol reverses the misfolding phenotype of the most common cystic fibrosis mutation. *J. Biol. Chem.* **271**:635–638.
46. Tamarappoo, B.K., Yang, B., and Verkman, A.S. 1999. Misfolding of mutant aquaporin-2 water channels in nephrogenic diabetes insipidus. *J. Biol. Chem.* **274**:34825–34831.
47. Tan, C.M., Nickols, H.H., and Limbird, L.E. 2003. Appropriate polarization following pharmacological rescue of V2 vasopressin receptors encoded by X-linked nephrogenic diabetes insipidus alleles involves a conformation of the receptor that also attains mature glycosylation. *J. Biol. Chem.* **278**:35678–35686.
48. Yang, Y., Janich, S., Cohn, J.A., and Wilson, J.M. 1993. The common variant of cystic fibrosis transmembrane conductance regulator is recognized by hsp70 and degraded in a pre-Golgi nonlysosomal compartment. *Proc. Natl. Acad. Sci. U. S. A.* **90**:9480–9484.
49. Rubenstein, R.C., and Zeitlin, P.L. 2000. Sodium 4-phenylbutyrate downregulates Hsc70: implications for intracellular trafficking of DeltaF508-CFTR. *Am. J. Physiol. Cell Physiol.* **278**:C259–C267.
50. Booth, C., and Koch, G.L. 1989. Perturbation of cellular calcium induces secretion of luminal ER proteins. *Cell.* **59**:729–737.
51. Rubenstein, R.C., Egan, M.E., and Zeitlin, P.L. 1997. In vitro pharmacologic restoration of CFTR-mediated chloride transport with sodium 4-phenylbutyrate in cystic fibrosis epithelial cells containing δ F508-CFTR. *J. Clin. Invest.* **100**:2457–2465.
52. Delisle, B.P., et al. 2003. Thapsigargin selectively rescues the trafficking defective LQT2 channels G601S and F805C. *J. Biol. Chem.* **278**:35749–35754.
53. Rubenstein, R.C., and Zeitlin, P.L. 1998. A pilot clinical trial of oral sodium 4-phenylbutyrate (Buphenyl) in deltaF508-homozygous cystic fibrosis patients: partial restoration of nasal epithelial CFTR function. *Am. J. Respir. Crit. Care Med.* **157**:484–490.
54. Zeitlin, P.L., et al. 2002. Evidence of CFTR function in cystic fibrosis after systemic administration of 4-phenylbutyrate. *Mol. Ther.* **6**:119–126.
55. Kausalya, P.J., Phua, D.C., and Hunziker, W. 2004. Association of ARVCF with zonula occludens (ZO)-1 and ZO-2: binding to PDZ-domain proteins and cell-cell adhesion regulate plasma membrane and nuclear localization of ARVCF. *Mol. Biol. Cell.* **15**:5503–5515.
56. Kausalya, P.J., Reichert, M., and Hunziker, W. 2001. Connexin45 directly binds to ZO-1 and localizes to the tight junction region in epithelial MDCK cells. *FEBS Lett.* **505**:92–96.
57. Schultz, S.G., and Zalusky, R. 1964. Ion transport in isolated rabbit ileum. Ii. The interaction between active sodium and active sugar transport. *J. Gen. Physiol.* **47**:1043–1059.
58. Müller, D., Kausalya, P.J., Meij, I.C., and Hunziker, W. 2006. Familial hypomagnesemia with hypercalciuria and nephrocalcinosis: blocking endocytosis restores surface expression of a novel Claudin-16 mutant that lacks the entire C-terminal cytosolic tail. *Hum. Mol. Genet.* In press.